energies

MDPI

Article

Neural Network Energy Management-Based Nonlinear Control of a DC Micro-Grid with Integrating Renewable Energies

Khalil Jouili [1], Mabrouk Jouili [2], Alsharef Mohammad [3], Abdulrahman J. Babqi [3] and Walid Belhadj [4,*]

[1] Laboratory of Advanced Systems, Polytechnic School of Tunisia (EPT), B.P. 743, Marsa 2078, Tunisia; khalil.jouili@ept.ucar.tn
[2] ETIS, CNRS UMR 8051, CY Cergy Paris University, ENSEA, 6 Avenue du Ponceau, 95014 Cergy, France; mabrouk.jouili@cyu.fr
[3] Department of Electrical Engineering, College of Engineering, Taif University, Taif 21944, Saudi Arabia; m.asharef@tu.edu.sa (A.M.); ajbabqii@tu.edu.sa (A.J.B.)
[4] Physics Department, Faculty of Science, Umm AL-Qura University, P.O. Box 715, Makkah 24382, Saudi Arabia
* Correspondence: wbbelhadj@uqu.edu.sa

Abstract: The broad acceptance of sustainable and renewable energy sources as a means of integrating them into electrical power networks is essential to promote sustainable development. Microgrids using direct currents (DCs) are becoming more and more popular because of their great energy efficiency and straightforward design. In this work, we discuss the control of a PV-based renewable energy system and a battery- and supercapacitor-based energy storage system in a DC microgrid. We describe a hierarchical control approach based on sliding-mode controllers and the Lyapunov stability theory. To balance the load and generation, a fuzzy logic-based energy management system has been created. Using a neural network, maximum power defects for the PV system were determined. The global asymptotic stability of the framework has been verified using Lyapunov stability analysis. In order to simulate the proposed DC microgrid and controllers, MATLAB/SimulinkR (2019a) was utilized. The outcomes show that the system operates effectively with changing production and consumption.

Keywords: renewable energy generation; DC microgrid; fuzzy logic system; sliding mode controller; Lyapunov stability

Citation: Jouili, K.; Jouili, M.; Mohammad, A.; Babqi, A.J.; Belhadj, W. Neural Network Energy Management-Based Nonlinear Control of a DC Micro-Grid with Integrating Renewable Energies. *Energies* **2024**, *17*, 3345. https://doi.org/10.3390/en17133345

Academic Editor: Tek Tjing Lie

Received: 2 June 2024
Revised: 29 June 2024
Accepted: 30 June 2024
Published: 8 July 2024

1. Introduction

The Distributed Generation concept has played an essential role in the transition from traditional power production to clean power energy over the last two decades. Wind and solar and energy are abundant across the world, and they are the primary contributors to decreasing carbon emissions and ensuring environmental sustainability [1,2]. They are used with REs and loads to build MGs. The major benefits of MGs are improved dependability, autonomous control, and the capacity to satisfy load needs in both grid-connected and islanded modes [3,4]. They are divided into two types, namely AC and DC. Because of their superior efficiency, lower cost, and lack of reactive power, DCMGs have been largely deployed in remote locations [5]. The MG requires an appropriate control strategy to deliver continuous and adequate energy for the load demand while balancing all power fluxes [6,7], and it may be linked to or disconnected from the main network. Because of its simplicity, linear control is the most commonly used technique for regulating MGs. It is also well known in both industry and academics. Significant studies have been performed to this end utilizing various linear control approaches. Complex optimization approaches were used to solve the DCMG's stability problem with constant power loads [8]. An observer-based droop control was used to manage the DC bus voltage of a simple MG with two storage units [9]. An expanded model for DG resources [10] was used to examine

a robust control approach for regulating energy units in a DCMG, with stability analysis being carried out using a defined set of eigen-values for a linearized model.

Research on the nonlinear nature of power converters integrated with DG units has been undertaken utilizing various linear control techniques [11,12], as well for nonlinear systems with fuzzy logic control [13]. Substantial research has been performed using the nonlinear control approaches to overcome the difficulties outlined in the case of linear control systems. The traditional MPPT method for PV array voltage was used to build a robust nonlinear controller for power source management in a DCMG with a PV solar panel [14]. A passivity-based nonlinear controller was investigated, and it was discovered that the bus voltage did not remain constant, and no global stability of the system was demonstrated [15]. The use of SE has been examined as a single DG unit using a nonlinear adaptive backstepping controller for islanded DCMGs [16]. A sliding mode nonlinear control has been examined in [17]; the variations' bus voltages were identified as a result of the lack of an ES device capable of providing quick energy transients under load demand. Considering the drawbacks of past studies and researching the control and operation of RESs coupled with storage energy systems, control is planned globally and implemented locally [18–20].

In order to overcome the difficulties faced by the aforementioned studies (among others), the MG is used in this study to integrate DG to time-varying demands, with storage system components operating on distinct time scales (battery and supercapacitor). The DCMG's control strategy is divided into two layers. The low-layer controller is based on the sliding-mode controller and Lyapunov stability, and ensures that each element is exponentially stable in relation to its own reference. Artificial neural networks are employed by the PV coupled with the MG to operate during MPPT, achieving optimum efficiency throughout the day despite disturbances from environmental changes.

Furthermore, high-level controllers based on fuzzy logic systems provide references based on various objectives, such as MPPT and maintaining the power equilibrium by delivering the desired currentof the battery and the reference current of SC, according to the load power needs. A constructive Lyapunov function explicitly analyzes the system's stability and ensures the exponential stability of the entire system under moderate conditions, which define the grid's operating conditions. The resulting system will then provide excellent dynamic performance and adaptability. Computer simulations are then used to validate the developed nonlinear control strategy.

The paper is structured as follows. Section 2 describes the system design and describes the DC microgrid model, Section 3 provides issue formulation and control goals, and Section 4 proposes an MPPT approach for the PV system, utilizing an artificial neural network. Section 5 analyzes the design of the proposed controller utilizing a fuzzy logic energy management system, and Section 6 investigates the stability analysis of the connected DC MG system. Section 7 contains the case studies and simulation results, followed by Section 8's conclusions

2. Components of DC Microgrid System

Figure 1 shows the DC microgrid system under examination. It is made up of a PV-generating source, a battery, and a supercapacitor energy storage unit that are all linked together by a Three-Input DC-DC Boost Converter. The PV input is connected to the DC microgrid by a single unidirectional leg, while the storage components are connected via two bidirectional legs. A power transmission line connects the load and DC bus.

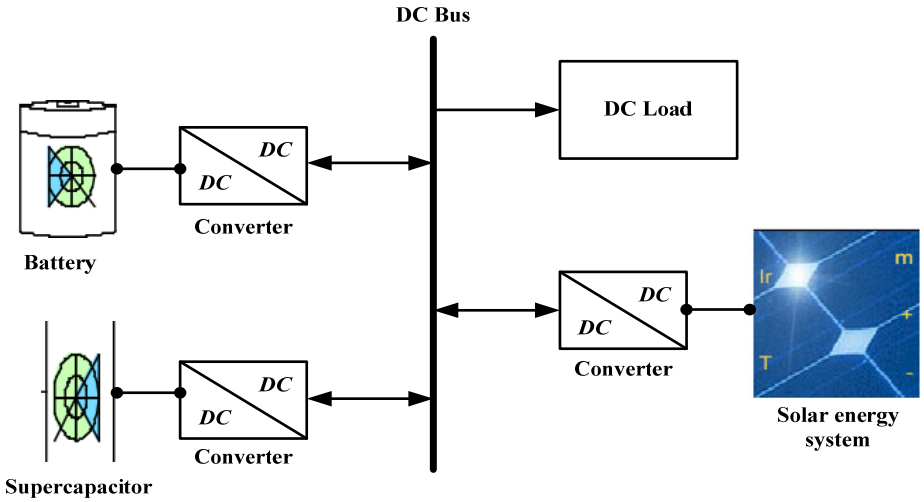

Figure 1. The DCMG system configuration.

2.1. PV Energy System

A solar panel is made up of PV modules, which absorb sunlight and convert it into direct current energy. Figure 2 depicts the layout of the PV energy system. The PV array was coupled to a DC-DC converter to exchange power with the DC bus, which was thought to be in continuous conduction mode. The system model requires two state variables in order to operate correctly as follows: The solar panel voltage is unknown, but the positive capacitance, resistance, and inductor values are known as C_1, R_1, R_{01}, R_{02}, L_1, respectively. The PV array voltage $V_{PV} \in \Re^+$ states I_{L1} and V_{C1} as the detected signals. The control input, u_1, is defined as the circuit's duty cycle; its objective is to properly integrate the power flowing from the source. This is referred to as MPPT, and it consists of regulating the voltage V_{C1} to its reference V_{C1ref}, which is provided by a higher-level controller and is supposed to remain constant across the time period T.

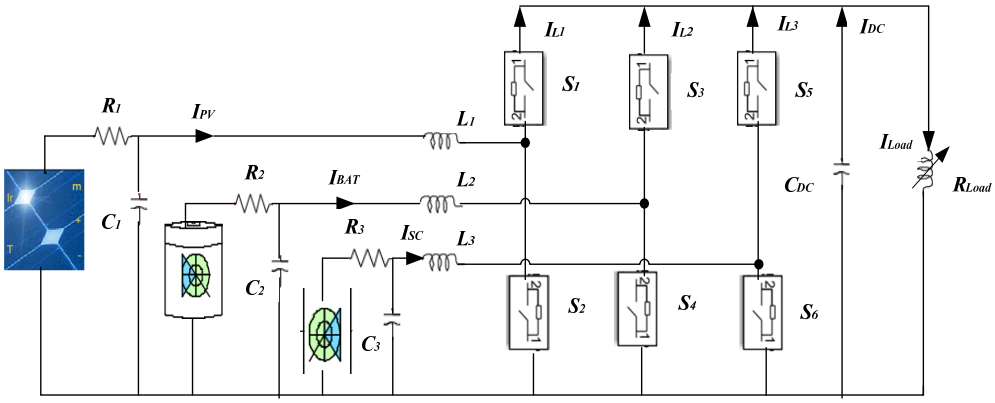

Figure 2. The circuit of DCMG system.

2.2. Battery Storage System

The battery is connected to the DC bus by the DC-DC converter. For the converter, we select two state variables as follows: the capacitor voltages V_{C2} and the inductor current I_{L2}. C_2, R_2, L_2, R_{03}, and R_{04} are well-known positive circuit variables, whereas the battery voltage is not. The signals monitored are the I_{L2} and V_{C2} states, as well as the battery voltage V_{BAT}. The duty cycle u_2 is used as the control input.

2.3. Supercapacitor Storage System

The SC is connected to the DC bus through the DC-DC converter. The inductor current I_{L3} and the capacitor voltage V_{C3} are significant. We know the positive values of C_3, R_3, L_3,

R_{05}, R_{06}, and the V_{SC} disturbance at each time t. (SC voltage). The system's control input is the duty cycle u_3. Its mission is to govern the V_{DC}. The voltage of a capacitor is directly linked to the grid. The observed signals are the SC voltage V_{SC}> 0, as well as the states V_{C3} and I_{L3}. In this case, V_{CD} indicates the voltage of the capacitor C_{CD}, which is the DCMG in Figure 2. This voltage is determined by the connections with the load and the sources, with $R_L \in \Re^+$ denoting the load resistance.

3. Problem Formulation and System Modeling

3.1. System Modeling

As shown in Figure 2, the mathematical model is obtained based on the power electronics averaging technique [21–23], controlled using PWM, and can be expressed using the following equations:

$$\begin{cases} \frac{dV_{C1}}{dt} = -\frac{1}{R_1C_1}V_{C1} - \frac{1}{C_1}I_{L1} + \frac{1}{R_1C_1}V_{PV} \\ \frac{dI_{L1}}{dt} = \frac{1}{L_1}V_{C1} - \frac{[(R_{01}-R_{02})u_1+R_{02}]}{L_1}I_{L1} - \frac{(1-u_1)}{L_1}V_{DC} \\ \frac{dV_{C2}}{dt} = -\frac{1}{R_2C_2}V_{C2} - \frac{1}{C_2}I_{L2} + \frac{1}{R_2C_2}V_{BAT} \\ \frac{dI_{L2}}{dt} = \frac{1}{L_2}V_{C2} - \frac{[(R_{03}-R_{04})u_2+R_{02}]}{L_2}I_{L2} - \frac{(1-u_2)}{L_2}V_{DC} \\ \frac{dV_{C3}}{dt} = -\frac{1}{R_3C_3}V_{C3} - \frac{1}{C_3}I_{L3} + \frac{1}{R_3C_3}V_{SC} \\ \frac{dI_{L3}}{dt} = \frac{1}{L_3}V_{C3} - \frac{[(R_{05}-R_{06})u_3+R_{06}]}{L_3}I_{L3} - \frac{(1-u_3)}{L_3}V_{DC} \\ \frac{dV_{DC}}{dt} = \frac{1}{C_{DC}}[(1-u_1)I_{L1} + I_{L2} + I_{L3} - i_{Load}] \end{cases} \quad (1)$$

Let $\begin{bmatrix} x_1 & x_2 & x_3 & x_4 & x_5 & x_6 & x_7 \end{bmatrix}^T = \begin{bmatrix} V_{C1} & I_{L1} & V_{C2} & I_{L2} & V_{C3} & I_{L3} & V_{DC} \end{bmatrix}^T$, then the system (1) can be rewritten as follows:

$$\begin{cases} \frac{dx_1}{dt} = -\frac{1}{R_1C_1}x_1 - \frac{1}{C_1}x_2 + \frac{1}{R_1C_1}V_{PV} \\ \frac{dx_2}{dt} = \frac{1}{L_1}x_1 - \frac{[(R_{01}-R_{02})u_1+R_{02}]}{L_1}x_2 - \frac{(1-u_1)}{L_1}x_7 \\ \frac{dx_3}{dt} = -\frac{1}{R_2C_2}x_3 - \frac{1}{C_2}x_4 + \frac{1}{R_2C_2}V_{BAT} \\ \frac{dx_4}{dt} = \frac{1}{L_2}x_3 - \frac{[(R_{03}-R_{04})u_2+R_{02}]}{L_2}x_4 - \frac{(1-u_2)}{L_2}x_7 \\ \frac{dx_5}{dt} = -\frac{1}{R_3C_3}x_5 - \frac{1}{C_3}x_6 + \frac{1}{R_3C_3}V_{SC} \\ \frac{dx_6}{dt} = \frac{1}{L_3}x_5 - \frac{[(R_{05}-R_{06})u_3+R_{06}]}{L_3}x_6 - \frac{(1-u_3)}{L_3}x_7 \\ \frac{dx_7}{dt} = \frac{1}{C_{DC}}[(1-u_1)x_2 + x_4 + x_6 - i_{Load}] \end{cases} \quad (2)$$

3.2. Analysis of the DCMG System

To understand the system's behavior, a thorough examination of the controller design necessary for DCMG control is carried out as follows:

3.2.1. Dynamical Behavior

The DCMG system includes a wide range of nonlinear dynamics due to the power sources and electromagnetic interactions between them, as well as numerous switching components exhibited in converters (boost-buck). Moreover, the dynamic characteristics of the converters has been categorized as including bifurcation and/or chaos [24,25]. To avoid the failure in the circuits, a mathematical modeling of the system has been suggested, while Lyapunov stability has been proven to be effective in regard to avoiding bifurcation.

3.2.2. Nonlinear Characteristics

The system is very nonlinear due to the interconnection and switching between the converters. Nonlinearity in converters may be addressed successfully using Lyapunov-based methods, which provide high sensitivity, robustness, and superior transient response [26].

3.2.3. Non-Minimum Phase Nature

The inductor shows this type of behavior when the current lags behind the desiredsignal in DC-DC converters [27]. The current's control systems, which utilize an indirect control method to force currents to follow their respective references, are used to prevent this tendency. The mentioned facts need the construction of a nonlinear controller capable of handling the nonlinear dynamic behavior of power converters. Furthermore, in the next section, the parameters of the proposed control strategy based on a nonlinear controller are built in such a way that they govern the nonlinearities.

3.3. Problem Formulation

The purpose of this work is to maintain the DCMG voltage at its nominal value, while also ensuring the total system's stability. The DCMG control is divided into two layers to achieve this goal.

3.3.1. High-Level Control

The PV high-level controller is based on an intelligent technology that uses an artificial neural network (ANN) [7] to harvest the most power from the solar panel. In DCMG, power flow management serves as a high-level controller for the storage system. The DCMG voltage V_{DC} is compared to its reference value V_{DCref}, and the total current required by the storage to fulfill the power flow and guide the DC grid voltage to its reference is calculated. To correct an equation, a Proportional Integral (*PI*) corrector is utilized. The objective of a fuzzy logic system (FLS) [28] is to generate the reference currents of a battery and a SC (I_{L2ref} and I_{L3ref}, respectively).

3.3.2. Low-Level Control

The control of power converters is required to regulate the input and output flow of the current based on reference signals provided by a sliding-mode control algorithm. Figure 3 shows the control approach and integration with a DC bus. The objective of this strategy is to stabilize the DCMG voltage and deliver adequate power to the load while decreasing battery charge/discharge cycles.

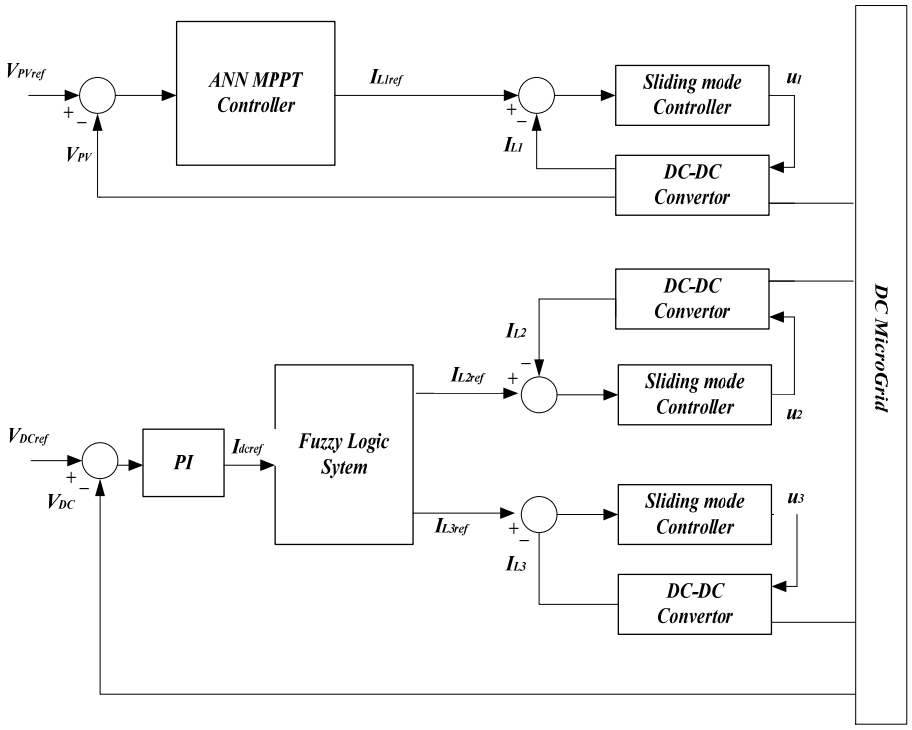

Figure 3. Block diagram of control strategy.

4. MPPT for a PV Subsystem Using Artificial Neural Network

To increase the capacity of a solar panel, its operating point must be controlled in order to obtain the maximum energy from it. This work optimized an artificial neural network MPPT controller to create the maximum peak power voltage, which delivers a reference voltage V_{C1ref} to be tracked by the lower level controller. Variations in meteorological conditions such as fog, heat, dust, and other particles floating in the air cover the panel over time, reducing the efficiency of the PV system's power conversion process significantly. Because the values generated by the neural network closely match the goal values, it may be used to estimate future indicator values of V_{C1ref} from previous data and to recognize trends in irradiance and temperature regardless of the variables indicated above. The data used to train and target the neural network was derived from a Simulink model of a PV array with variable temperature and irradiance data points.

As illustrated in Figure 4, the neural network described in this workhas two inputs, temperature and solar irradiance, and one output, V_{C1ref}.

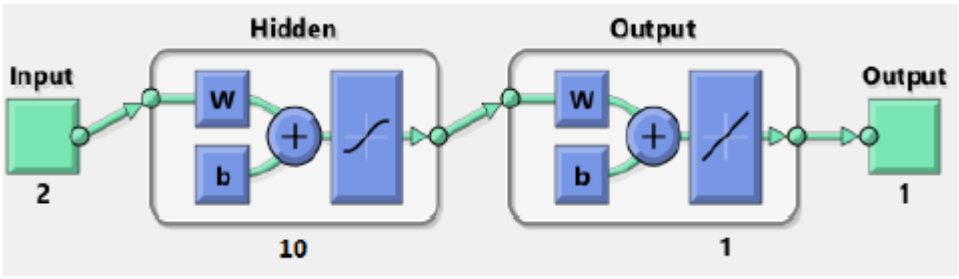

Figure 4. Matlab ANN architecture proposed for MPPT.

The number of neurons in the hidden layer has been used to regulate the network's performance. The input data have been sent to the hidden layers, which have calculated the output data. To train the neural network, the Levenberg–Marquardt method [7] was used to solve nonlinear issues, such as fluctuations in irradiance and temperature. The regression plot constructed using the neural network toolbox in MATLAB (2019a), displayed in Figure 5, shows that the output value of V_{C1ref} accurately reflects the target data. The solid line in the regression plot indicates the perfect correlation between the predicted and target data, while the dashed line represents the best fit provided by the neural network method.

Table 1 shows a comparison between V_{C1ref} target values and neural network-produced values. The findings of the artificial neural network MPPT controller provide reliable forecasts throughout a wide range of operating modes, particularly for very rapid changes in weather conditions, which produces a reference voltage V_{C1ref}.

Table 1. A comparison of the V_{C1ref}'s trained and simulated values.

G (w/m^2)	T(°C)	V_{C1ref}(V)	
		Trained	Simulated Value
640	21	294.2523	293.385
700	26	287.681	286.163
500	31.6	280.308	281.629
900	37.4	272.673	270.944
1000	42	266.610	266.713
855	36	274.654	273.496
740	33	278.496	278.911
615	30	282.472	281.911
515	27.2	286.177	287.385
445	25	289.085	288.219

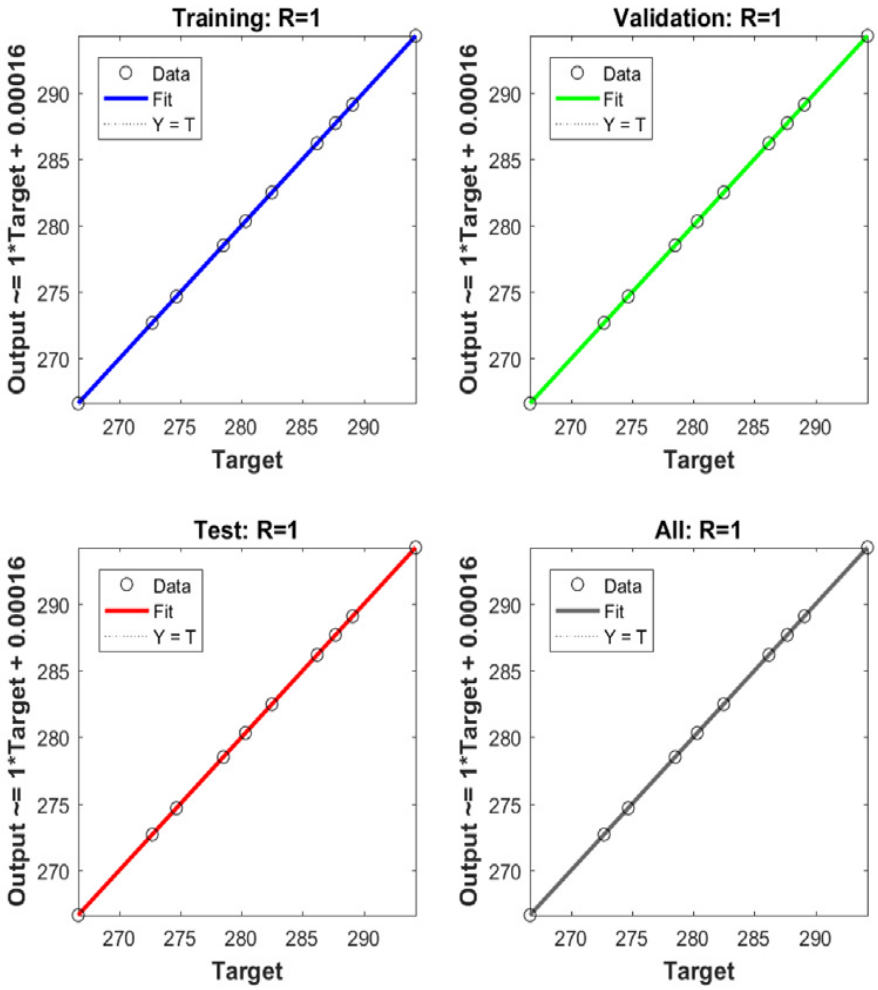

Figure 5. Regression plot using for the ANN.

5. DC Microgrid Control and FLS Energy Management

5.1. Fuzzy Logic Energy Management System

The artificial neural network MPPT controller provides a reference voltage V_{C1ref} that the lower level controller may track. A Li-ion battery and a SC are employed in the proposed storage system. The control's goal is to charge and discharge the storage component while maintaining a steady grid voltage during transients. The current going from/to the storage to/from the DC-link capacitance represents the power necessary to complete the power flow. Due to the buck-boost converter's non-minimum phase behavior, the DC bus voltage V_{DC} cannot be set directly to V_{DCref}. To keep the bus voltage at the reference voltage V_{DCref}, the *PI* corrector calculates the DC bus reference current I_{dcref}.

The FLS (Figure 6) delivers the battery and SC reference currents (I_{L2ref} and I_{L3ref}, respectively). These reference currents will allow the DC bus voltage to stay constant regardless of the load behavior or variations in the PV generator power drawn.

To divert unexpected power variations into the SC, a low-pass filter is applied to the I_{dc} current. The I_{dcref} current is transmitted through this low filter to create the battery's current desired I_{dcref}. The difference between the I_{dcref} and $I_{L2ref}{}'$ determines the SC current reference $I_{L3ref}{}'$.

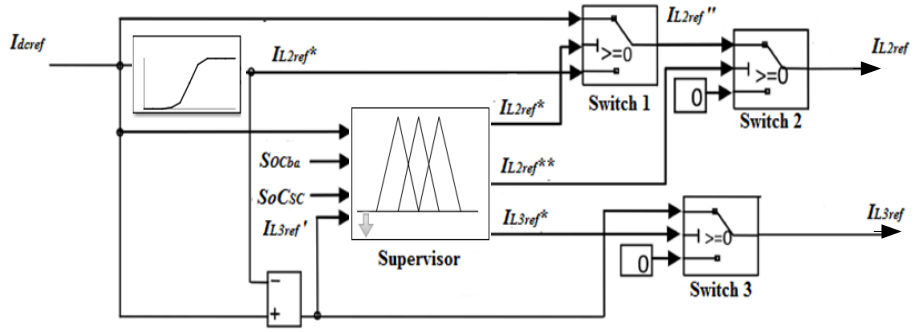

Figure 6. A block diagram demonstrating the fuzzy logic system.

The *SoC* of the battery and the SC must be considered while developing the reference currents. To choose the exact reference current, three switches are utilized, which are controlled by the FLS in function of I_{L2ref}*, I_{L2ref}**, and I_{L3ref}*.

***Switch 1*:** Lets you choose between I_{dcref} and $I_{L2ref}{}'$.
If I_{dcref} is Negative and SoC_{SC} is 95%, $I_{L2ref}{}''$ equals I_{dcref}; else, $I_{L2ref}{}''$ equals $I_{L2ref}{}'$.
If I_{dcref} is Positive and SoC_{SC} is 25%, $I_{L2ref}{}''$ equals I_{dcref}; else, $I_{L2ref}{}''$ equals $I_{L2ref}{}'$.
***Switch 2*:** Lets you to choose between $I_{L2ref}{}''$ and 0.
If I_{dcref} is Negative and SoC_{ba} is 95%, I_{L2ref} equals zero; else, I_{L2ref} equals $I_{L2ref}{}''$.
If $I_{L2ref}{}''$ is Positive and SoC_{ba} is 25%, I_{L2ref} equals zero; else, I_{L2ref} equals $I_{L2ref}{}''$.
***Switch 3*:** Lets you choose between $I_{L3ref}{}'$ and 0.
If $I_{L3ref}{}'$ is Negative and SoC_{SC} is 95%, I_{L3ref} equals zero; else, I_{L3ref} equals $I_{L3ref}{}'$.
If $I_{L3ref}{}'$ is Positive and SoC_{SC} is 25%, I_{L3ref} equals zero; else, I_{L3ref} equals $I_{L3ref}{}'$.

- If the storge reference currentI_{L2ref} is Negative, then the PV generator will produce greater power than the load and the *SoC* of SC is greater that 95%, meaning the I_{L3ref} must be null.
- If the storge reference current I_{L2ref} is positive, then the PV generator will fail to deliver sufficient power and the *SoC* of SC is 25%, meaning the I_{L3ref} must be null.
- If the Supercapacitor's SoC exceeds 25%, the SC will start to discharge.
- When the PV panels supply the power required by the load, the I_{DCref} is zero.

The aim of utilizing a FLS in this study is to regulate the total system power flow while keeping the SoC_{ba} and the SoC_{SC} at their allowable intervals of their *SoC*. As illustrated in Figures 7 and 8, the FLS employed in this work comprises four inputs and three outputs.

The fuzzy logic system's inputs are the storage reference current I_{dcref}, the SoC_{ba}, the SoC_{SC}, and I_{L3ref}.

The outputs are I_{L2ref}* for the control of *switch 1*, I_{L2ref}**for the control of *switch 2*, and I_{L3ref}* for the control of *switch 3*.

The FLS calculates the control of the three switches utilized for DC bus regulation using the data from these four inputs, as shown in the flowchart.

Membership functions:

The described methodology's objective is to develop membership functions for the FLS's input and output variables. The input membership functions are used to switch between the various operational modes. Figures 7 and 8 depict them. To accommodate the needs of the proposed strategy, the membership functions of the storage levels (Figure 7a,d) are based on two levels; N stands for negative, and P stands for positive, where they represent the sign of the reference current I_{dcref} and $I_{L3ref}{}'$,with N and P representing the charge and discharge of the SC and battery, respectively. Between 100 and −100 A, the reference currents $I_{L3ref}{}'$ and I_{dcref} are considered.

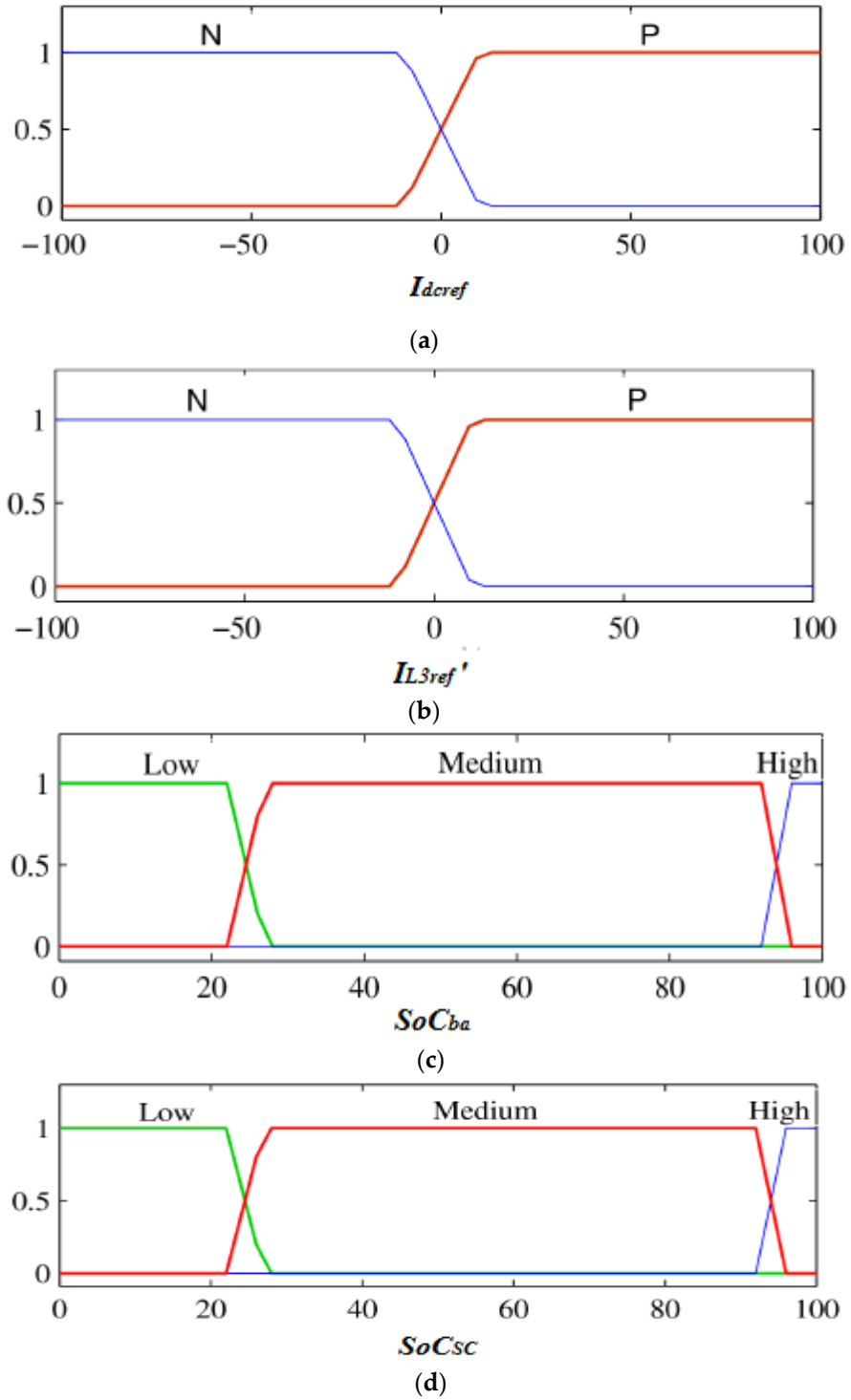

Figure 7. Inputs of the fuzzy logic system. (**a**) Membership functions of I_{dcref}, (**b**) membership functions of $I_{L3ref}{}'$, (**c**) membership functions of $SoC_{ba,}$ and (**d**) membership functions of SoC_{SC}.

The described methodology's objective is to develop membership functions for the inputs and outputs variables of the FLS. The membership functions are employed to switch between the various operational modes. Figures 5 and 6 depict them. To satisfy the demands of the suggested approach, the membership functions are based on two levels, N and P (Figure 7a–d).

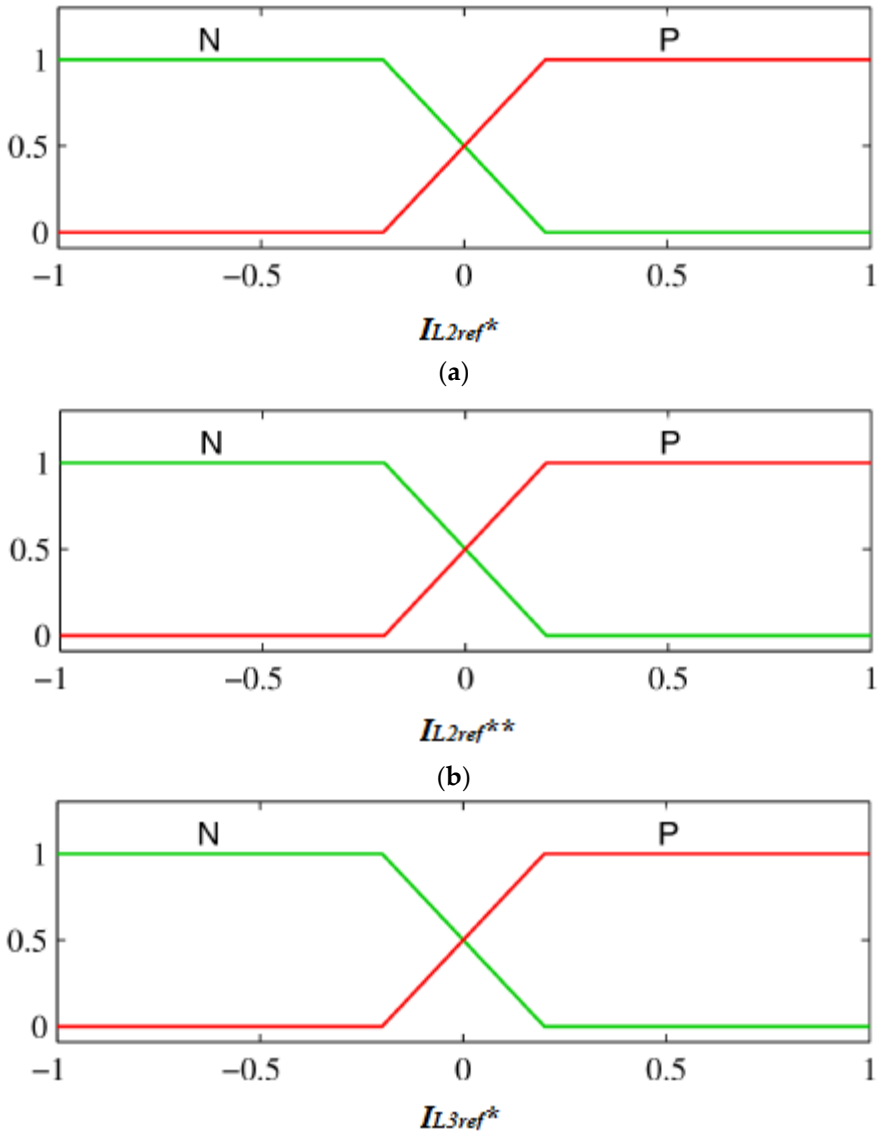

Figure 8. Outputs of the fuzzy logic system. (**a**) Membership functions of I_{L2ref}*, (**b**) membership functions of I_{L2ref}**, and (**c**) membership functions of I_{L3ref}*.

The membership of the SoC_{ba} and the SoC_{SC} is depicted in Figure 7b,c. Similarly, three levels are defined as follows:

- The *SoC* is represented by a low level of 25% (between 0 and 25%).
- The *SoC* is represented by a middling level of 25 to 95%.
- The *SoC* is represented at a high level of >95%.

The membership functions of the outputs are illustrated in Figure 8a–c, with switch1 controlling I_{L2ref}*, switch2 controlling I_{L2ref}**, and switch 3 controlling I_{L3ref}*. These functions are divided into two tiers, N and P, which indicate the sign of the switch commands.

Rules of FLS:

The rules of the FLS generated for energy management storage are derived from system behavior analysis. It must be recognized in their formulation that utilizing different control rules based on operational situations might increase the performance of the energy management storage. The rules that link the FLS are shown in the following tables (Tables 2–4):

Table 2. Rules of the current I_{L2ref}*.

		SoC_{ba}		
		Low	**Medium**	**High**
I_{dcref}	N	P	P	N
	P	N	P	P

Table 3. Rules of the current I_{L2ref}**.

		SoCsc		
		Low	**Medium**	**High**
I_{dcref}	N	P	P	N
	P	N	P	P

Table 4. Rules of the current I_{L3ref}*.

		SoCsc		
		Low	**Medium**	**High**
$I_{dcref}{}'$	N	P	P	N
	P	N	P	P

5.2. PV Subsystem Controller

Lets us look at the control u_1 that is used to stabilizex_1 and x_2; it is created via utilizing a sliding-mode approach to create an x_{1ref} desiredvalue to x_1 that is employed to guide V_{C1} to its equilibrium point after imposing a desirable dynamic behavior. From system (2),

$$\begin{cases} \frac{dx_1}{dt} = -\frac{1}{R_1C_1}x_1 - \frac{1}{C_1}x_2 + \frac{1}{R_1C_1}V_{PV} \\ \frac{dx_2}{dt} = \frac{1}{L_1}x_1 - \frac{[(R_{01}-R_{02})u_1+R_{02}]}{L_1}x_2 - \frac{(1-u_1)}{L_1}x_7 \end{cases} \tag{3}$$

Let us first establish the output tracking error as $e_1 = x_1 - x_{1ref}$; the control input's u_1 goal is to correctly incorporate the PV energy while also obtaining the maximum power possible from the PV generator. This is known as MPPT, and it consists of regulating the voltage V_{C1} (x_1) to its reference V_{C1ref} (x_{1ref}) delivered by a higher-level controller and deemed constant throughout each time period T. The desired dynamic for x_1 is introduced as

$$\dot{e}_1 = \dot{x}_1 - \dot{x}_{1ref} \tag{4}$$

From Equations (3)and (4), we can then design

$$x_{2ref} = \frac{1}{R_1}\left[V_{PV} - x_{1ref}\right] \tag{5}$$

To track the state x_2 to its reference value x_{2ref}, we establish the following error term for the controller's design:

$$e_2 = x_2 - x_{2ref} \tag{6}$$

To develop an SMC, an SF was chosen that allows the system to reach the SF and achieve the required desired value. Since the PV energy subsystem's state space model has just only one control law input u_1, the SF has been defined as follows:

$$S_2 = a_2\left(x_2 - x_{2ref}\right) = a_2e_2 \tag{7}$$

where a_2 is a positive constant for the SF design parameter. If we derive the time of Equation (7), we obtain the following:

$$\dot{S}_2 = a_2\left(\dot{x}_2 - \dot{x}_{2ref}\right) = a_2\dot{e}_2 \tag{8}$$

Equation (6)'s time derivative provides the following equation:

$$\dot{e}_2 = \dot{x}_2 - \dot{x}_{2ref} \tag{9}$$

Replacing $\dot{x}_2$ from Equation (3) into Equation (9) yields

$$\dot{e}_2 = \frac{1}{L_1}x_1 - \frac{[(R_{01} - R_{02})u_1 + R_{02}]}{L_1}x_2 - \frac{(1-u_1)}{L_1}x_7 - \dot{x}_{2ref} \tag{10}$$

Substituting $\dot{e}_2$ from Equation (10) into Equation (8) yields

$$\dot{S}_2 = a_2\left[\frac{1}{L_1}x_1 - \frac{[(R_{01} - R_{02})u_1 + R_{02}]}{L_1}x_2 - \frac{(1-u_1)}{L_1}x_7 - \dot{x}_{2ref}\right] \tag{11}$$

The control law u_1 was selected in a manner so that it achieves global asymptotic stability, as indicated below:

$$u_1 = u_{SC1} + u_{NC1} \tag{12}$$

where u_{SC1} denotes the switching control that keeps the track on the SF and u_{NC1} denotes the nominal control that brings the trajectory state to the SF. Using $\dot{S}_2 = 0$ to obtain the value of u_{NC1} yields

$$u_{NC1} = \frac{a_2 L_1}{(R_{01} - R_{02})x_2 - x_7}\left[\frac{1}{L_1}x_1 - \frac{1}{L_1}x_7 - \frac{R_{02}}{L_1}x_2 - \dot{x}_{2ref}\right] \tag{13}$$

and

$$u_{SC1} = \frac{L_1}{(R_{02} - R_{01})x_2 + x_7}\left[-k_1|S_2|^{\alpha}sgn\left(\frac{S_2}{\phi_1}\right) - k_2\int sgn\left(\frac{S_2}{\phi_1}\right)dt\right] \tag{14}$$

In Equations (13) and (14), the condition (always met in practice) $(R_{01} - R_{02})x_2 - x_7 \neq 0$, α is a constant ranging from 0 to 1 that converges the subsystem (3) to the SF, ϕ_1 is the degree of nonlinearity used to prevent chattering, and k_1 and k_2 are gains (positive) that are used to modify the control law u_1. *Sgn* is the Signumfunction, which is in the following form:

$$sgn(S) = \begin{cases} -1 \ if \ S \leq 0 \\ 0 \ if \ S = 0 \\ 1 \ if \ S > 0 \end{cases} \tag{15}$$

Substituting the value of u_1 in (12), (13), and (14) results in the following:

$$\dot{S}_2 = -k_1|S_2|^{\alpha}sgn\left(\frac{S_2}{\phi_1}\right) - k_2\int sgn\left(\frac{S_2}{\phi_1}\right)dt \tag{16}$$

For stability analysis, rearrange (16) as follows:

$$\dot{S}_2 = w_2 + z_2 \tag{17}$$

where $w_2 = -k_1|S_2|^{\alpha}sgn\left(\frac{S_2}{\phi_1}\right)$ and $\dot{z}_2 = -k_2 sgn\left(\frac{S_2}{\phi_1}\right)$.

To evaluate the subsystem's (2) stability, the following Lyapunov candidate function was used:

$$V_{1,2}(x) = 2k_2|S_2| + \frac{1}{2}z_2^2 + \frac{1}{2}\left(k_1|S_2|^{\alpha}sgn\left(\frac{S_2}{\phi_1}\right) - z_2\right)^2 + \frac{R_1}{2}e_1^2 \tag{18}$$

The Lyapunov function in (18) has a quadratic form as follows:

$$V_{1,2}(x) = X_1^T P_1 X_1 + X_2^T P_2 X_2 \tag{19}$$

where $X_1^T = \begin{bmatrix} e_1 & 0 \end{bmatrix}$, $X_2^T = \begin{bmatrix} |S_2|^{\alpha} sgn\left(\frac{S_2}{\phi_1}\right) & z_2 \end{bmatrix}$, $P_1 = \frac{R_1}{2}\begin{bmatrix} 1 & 0 \\ 0 & 0 \end{bmatrix}$, and $P_2 = \frac{1}{2}\begin{bmatrix} 4k_2 + k_1^2 & -k_1 \\ -k_1 & 2 \end{bmatrix}$.

Its time derivative along the solution of (16) yields the following results:

$$\dot{V}_{1,2}(x) = -\frac{1}{2|S_2|^{\alpha}} X_{1,2}^T Q_{1,2} X_{1,2} \tag{20}$$

where k_1 and k_2 are positive and $Q_{1,2} = \frac{k_2}{2}\begin{bmatrix} 2k_2 + k_1^2 + \frac{2}{k_2} & -k_1 \\ -k_1 & 1 \end{bmatrix}$.

In this case, if the controller gains k_1 and k_2 are positive, then $Q_{1,2} > 0$. The controller u_1 fits the Lyapunov stability condition, as demonstrated by (18), ensuring that the error convergence is zero in the limited time. It also shows that the PV subsystem can provide maximum power throughout the day.

$$\dot{V}_{1,2}(x) \leq 0 \tag{21}$$

5.3. Design of the Battery's Current Control

We must create a control law u_2 to direct I_{L2} toward its reference $x_{4ref} = I_{L2ref}$. It is developed using a sliding-mode technique. From system (1),

$$\begin{cases} \dfrac{dx_4}{dt} = \dfrac{1}{L_2} x_3 - \dfrac{[(R_{03} - R_{04})u_2 + R_{02}]}{L_2} x_4 - \dfrac{(1 - u_2)}{L_2} x_7 \end{cases} \tag{22}$$

To track the state x_4 to its referencevalue x_{4ref}, we establish the following error term for the controller's design:

$$e_4 = x_4 - x_{4ref} \tag{23}$$

To develop an SMC, an SF was chosen that allows the system to reach the SF and achieve the required desired value. Since the current battery subsystem's state space model just has only one control law input u_2, the SF has been defined as follows:

$$S_4 = a_4\left(x_4 - x_{4ref}\right) = a_4 e_4 \tag{24}$$

where a_4 is a positive constant for the SF design parameter. We derive the time of Equation (24), obtaining the following:

$$\dot{S}_4 = a_4\left(\dot{x}_4 - \dot{x}_{4ref}\right) = a_4 \dot{e}_4 \tag{25}$$

Equation (23)'s time derivative provides the following equation:

$$\dot{e}_4 = \dot{x}_4 - \dot{x}_{4ref} \tag{26}$$

Substituting the value of $\dot{x}_4$ from Equation (22) into Equation (26) yields

$$\dot{e}_4 = \frac{1}{L_2} x_3 - \frac{[(R_{03} - R_{04})u_2 + R_{02}]}{L_2} x_4 - \frac{(1 - u_2)}{L_2} x_7 - \dot{x}_{4ref} \tag{27}$$

Substituting $\dot{e}_4$ from Equation (27) into Equation (25) yields

$$\dot{S}_4 = a_4\left[\frac{1}{L_2} x_3 - \frac{[(R_{03} - R_{04})u_2 + R_{04}]}{L_2} x_4 - \frac{(1 - u_2)}{L_2} x_7 - \dot{x}_{4ref}\right] \tag{28}$$

The control law u_2 was selected in a manner that achieves global asymptotic stability, as indicated below:

$$u_2 = u_{SC2} + u_{NC2} \tag{29}$$

where u_{SC2} denotes the switching control that keeps the track on the SF and u_{NC2} denotes the nominal control that brings the trajectory state to the SF. Using $\dot{S}_4 = 0$ to obtain the value of u_{NC2} yields

$$u_{NC2} = \frac{a_4 L_2}{(R_{03} - R_{04})x_4 - x_7}\left[\frac{1}{L_2}x_3 - \frac{1}{L_2}x_7 - \frac{R_{04}}{L_2}x_4 - \dot{x}_{4ref}\right] \tag{30}$$

and

$$u_{SC2} = \frac{L_2}{(R_{04} - R_{03})x_4 + x_7}\left[-k_3|S_4|^{\beta}sgn\left(\frac{S_4}{\phi_2}\right) - k_4\int sgn\left(\frac{S_4}{\phi_2}\right)dt\right] \tag{31}$$

In Equations (30) and (31), the condition (always met in practice) $(R_{04} - R_{03})x_4 + x_7 \neq 0$, β is a constant ranging from 0 to 1 which converges the subsystem (22) to the SF, ϕ_2 is the degree of nonlinearity used to prevent chattering, and, k_3 and k_4 are gains (positive) that are used to modify the control law u_2. Substituting the value of u_2 in (29), (30), and (31) results in the following:

$$\dot{S}_4 = -k_3|S_4|^{\beta}sgn\left(\frac{S_4}{\phi_2}\right) - k_4\int sgn\left(\frac{S_4}{\phi_2}\right)dt \tag{32}$$

For stability analysis, rearrange (32) as follows:

$$\dot{S}_4 = w_4 + z_4 \tag{33}$$

where $w_4 = -k_4|S_4|^{\beta}sgn\left(\frac{S_4}{\phi_2}\right)$ and $\dot{z}_4 = -k_4 sgn\left(\frac{S_4}{\phi_2}\right)$.

To evaluate the system's stability, the following Lyapunov candidate function was used:

$$V_4(x) = 2k_4|S_4| + \frac{1}{2}z_4^2 + \frac{1}{2}\left(k_3|S_4|^{\beta}sgn\left(\frac{S_4}{\phi_2}\right) - z_4\right)^2 \tag{34}$$

The Lyapunov function in (34) has a quadratic form $V_4(x) = X_4^T P_4 X_4$, where

$$X_4^T = \begin{bmatrix}|S_4|^{\beta}sgn\left(\frac{S_4}{\phi_2}\right) & z_4\end{bmatrix} \tag{35}$$

and

$$P_4 = \frac{1}{2}\begin{bmatrix}4k_4 + k_3^2 & -k_3\\ -k_3 & 2\end{bmatrix} \tag{36}$$

Its time derivative along the solution of (34) yields the following results:

$$\dot{V}_4(x) = -\frac{1}{2|S|^{\beta}}X_4^T Q_4 X_4 \tag{37}$$

where k_3 and k_4 are positive and $Q_4 = \frac{k_4}{2}\begin{bmatrix}2k_4 + k_3^2 & -k_3\\ -k_3 & 1\end{bmatrix}$.

In this case, if the controller gains k_3 and k_4 are positive, then $Q_4 > 0$.

The controller u_2 fits the Lyapunov stability condition, as demonstrated by (38), ensuring that the error convergence is zero in the limited time. This controller guarantees that the battery is effectively managed and that the DCMG operates consistently under different load situations.

$$\dot{V}_4(x) \leq 0 \tag{38}$$

5.4. Control Law Design for Supercapacitor

We must design a control law u_3 to control the dynamics I_{L3} to ensure that the supercapacitor charges and discharges as required. It is developed using a sliding-mode technique. From system (1),

$$\begin{cases} \dfrac{dx_6}{dt} = \dfrac{1}{L_3}x_5 - \dfrac{[(R_{05}-R_{06})u_3 + R_{06}]}{L_3}x_6 - \dfrac{(1-u_3)}{L_3}x_7 \end{cases} \tag{39}$$

To track the state x_6 to its referencevalue x_{6ref}, we establish the following error term for the controller's design:

$$e_6 = x_6 - x_{6ref} \tag{40}$$

To develop an SMC, an SF was chosen that allows the system to reach the SF and achieve the required desired value. Since the current supercapacitor subsystem's state space model has only one control law input u_3, the SF has been defined as follows:

$$S_6 = a_6\left(x_6 - x_{6ref}\right) = a_6 e_6 \tag{41}$$

where a_3 is a positive constant for the SF design parameter. We derive the time of Equation (41), obtaining

$$\dot{S}_6 = a_6\left(\dot{x}_6 - \dot{x}_{6ref}\right) = a_6\dot{e}_6 \tag{42}$$

Equation (40)s' time derivative provides the following equation:

$$\dot{e}_6 = \dot{x}_6 - \dot{x}_{6ref} \tag{43}$$

Substituting the value of $\dot{x}_6$ from Equation (39) into Equation (43) yields

$$\dot{e}_6 = \frac{1}{L_3}x_5 - \frac{[(R_{05}-R_{06})u_3 + R_{06}]}{L_3}x_6 - \frac{(1-u_3)}{L_3}x_7 - \dot{x}_{6ref} \tag{44}$$

Substituting $\dot{e}_6$ from Equation (44) into Equation (42) yields

$$\dot{S}_6 = a_6\left[\frac{1}{L_3}x_3 - \frac{[(R_{05}-R_{06})u_3 + R_{06}]}{L_3}x_4 - \frac{(1-u_3)}{L_3}x_7 - \dot{x}_{6ref}\right] \tag{45}$$

The control law u_3 was selected in a manner that achieves global asymptotic stability, as indicated below:

$$u_3 = u_{SC3} + u_{NC3} \tag{46}$$

where u_{SC3} denotes the switching control that keeps the track on the SF and u_{NC1} denotes the nominal control that brings the trajectory state to the SF. Using $\dot{S}_6 = 0$ to obtain the value of u_{NC3} yields

$$u_{NC3} = \frac{a_6 L_3}{(R_{05}-R_{06})x_6 - x_7}\left[\frac{1}{L_3}x_5 - \frac{1}{L_3}x_7 - \frac{R_{06}}{L_3}x_6 - \dot{x}_{6ref}\right] \tag{47}$$

and

$$u_{SC3} = \frac{L_3}{(R_{05}-R_{06})x_6 + x_7}\left[-k_5|S_6|^{\delta}sgn\left(\frac{S_4}{\phi_3}\right) - k_6\int sgn\left(\frac{S_6}{\phi_3}\right)dt\right] \tag{48}$$

In Equations (47) and (48), the condition (always met in practice) $(R_{05}-R_{06})x_6 + x_7 \neq 0$, δ is a constant ranging from 0 to 1 that converges the subsystem (39) to the SF, ϕ_3 is the degree of nonlinearity used to prevent chattering, and k_1 and k_2 are gains (positive) that are used to modify the control law u_3. Substituting the value of u_3 in (46), (47), and (48) results in the following:

$$\dot{S}_6 = -k_5|S_6|^{\delta}sgn\left(\frac{S_6}{\phi_3}\right) - k_6\int sgn\left(\frac{S_6}{\phi_3}\right)dt \tag{49}$$

For stability analysis, rearrange (49) as follows:

$$\dot{S}_6 = w_6 + z_6\dot{S}_6 = w_6 + z_6 \tag{50}$$

where $w_6 = -k_6|S_6|^{\delta}sgn\left(\frac{S_6}{\phi_3}\right)$ and $\dot{z}_6 = -k_6 sgn\left(\frac{S_6}{\phi_3}\right)$.

To evaluate the system's stability, the following Lyapunov candidate function was used:

$$V_6(x) = 2k_6|S_6| + \frac{1}{2}z_6^2 + \frac{1}{2}\left(k_5|S_6|^{\delta}sgn\left(\frac{S_6}{\phi_3}\right) - z_6\right)^2 \tag{51}$$

The Lyapunov function in (51) has a quadratic form $V_6(x) = X_6^T P_6 X_6$,where

$$X_6^T = \begin{bmatrix} |S_6|^{\delta}sgn\left(\frac{S_6}{\phi_3}\right) & z_6 \end{bmatrix} \tag{52}$$

and

$$P_6 = \frac{1}{2}\begin{bmatrix} 4k_6 + k_5^2 & -k_5 \\ -k_5 & 2 \end{bmatrix} \tag{53}$$

Its time derivative along the solution of (51) yields the following results:

$$\dot{V}_6(x) = -\frac{1}{2|S|^{\delta}}X_6^T Q_6 X_6 \tag{54}$$

where k_5 and k_6 are positive and $Q_6 = \frac{k_6}{2}\begin{bmatrix} 2k_6 + k_5^2 & -k_5 \\ -k_5 & 1 \end{bmatrix}$.

In (54), P_6 is a positive definite matrix with positive k_5 and k_6 values. By carrying out the Lyapunov function stability analysis as described in the preceding paragraph, it is possible to deduce that the control law u_3 renders the subsystem (39) asymptotically stable, as demonstrated by (55). These controllers guarantee that the supercapacitor is effectively managed and that the DCMG operate consistently under different load situations.

$$\dot{V}_6(x) \leq 0 \tag{55}$$

6. Interconnected System Stability Analysis

In the previous section, we designed the decentralized nonlinear controllers based on the sliding mode for the controlled variable states x_1, x_2, x_4, x_6, and x_7, which represent photovoltaic, battery, and supercapacitor energy systems with the FLS-based power management system, which has been proposed for sharing load demands and to stabilize the V_{DC} voltage of the DC bus directly to V_{DCref}.

However, for the uncontrolled variables, V_{C2} (x_3) and V_{C3} (x_5) cannot be directly controlled due to non-minimum phase behavior (zero-dynamics); regulation is only valid when the system is operating near its steady state operating point or in a neighborhood of equilibrium.

Let us now shift our consideration to the internal dynamics (zero-dynamics). The zero-dynamics equations of DCMG-system (1) may be rewritten as follows:

$$\begin{cases} \frac{dx_3}{dt} = -\frac{1}{R_2C_2}x_3 - \frac{1}{C_2}x_4 + \frac{1}{R_2C_2}V_{BAT} \\ \frac{dx_5}{dt} = -\frac{1}{R_3C_3}x_5 - \frac{1}{C_3}x_6 + \frac{1}{R_3C_3}V_{SC} \end{cases} \tag{56}$$

The equilibrium $V_{C2}^e\left(x_3^e\right)$ and $V_{C3}^e\left(x_5^e\right)$ can be yielded by computing the nonlinear system of Equation (56) $\left(\frac{dx_3}{dt} = 0\frac{dx_5}{dt} = 0\right)$ as follows:

$$\begin{cases} 0 = -\frac{1}{R_2C_2}x_3 - \frac{1}{C_2}x_{4ref} + \frac{1}{R_2C_2}V_{BAT} \\ 0 = -\frac{1}{R_3C_3}x_5 - \frac{1}{C_3}x_{6ref} + \frac{1}{R_3C_3}V_{SC} \end{cases} \tag{57}$$

In fact, a direct calculation gives

$$\begin{cases} x_3^e = R_2C_2\left[-\frac{1}{C_2}x_{4ref} + \frac{1}{R_2C_2}V_{BAT}\right] \\ x_5^e = R_3C_3\left[-\frac{1}{C_3}x_{6ref} + \frac{1}{R_3C_3}V_{SC}\right] \end{cases} \tag{58}$$

As a result, a distinct equilibrium $x^e = \begin{bmatrix} x_{1ref} & x_{2ref} & x_3^e & x_{4ref} & x_5^e & x_{1ref} & x_{1ref} \end{bmatrix}^T$ of system (1) may be found. The errors e_3 and e_5 are defined as follows:

$$\begin{cases} e_3 = \left(x_3 - x_3^e\right) \\ e_5 = \left(x_5 - x_5^e\right) \end{cases} \tag{59}$$

The following Lyapunov function $V_{3,5}(x)$ is proposed:

$$V_{3,5}(x) = e_3^T P_3 e_3 + e_5^T P_5 e_5 \tag{60}$$

where $P_3 = \frac{R_2C_2}{2}\begin{bmatrix} 1 & 0 \\ 0 & 0 \end{bmatrix}$ and $P_5 = \frac{R_3C_3}{2}\begin{bmatrix} 1 & 0 \\ 0 & 0 \end{bmatrix}$.

Its time derivative yields the following results:

$$\dot{V}_{3,5}(x) = -e_3^2 - e_5^2 \tag{61}$$

The Lyapunov function's derivative $\dot{V}_{3,5}(x)$ is negative definite, ensuring the zero dynamics' exponential stability.

These partial conclusions may now be grouped together in the following theorem, which establishes the total stability characteristic.

Theorem 1. *Considering the DCMG system (1) and the equilibrium points that it has established,* $x^e = \begin{bmatrix} x_{1ref} & x_{2ref} & x_3^e & x_{4ref} & x_5^e & x_{1ref} & x_{1ref} \end{bmatrix}^T$*, assuming that the following conditions are met each time:*

$$\begin{cases} (R_{01} - R_{02})x_2 - x_7 \neq 0 \\ (R_{03} - R_{04})x_4 - x_7 \neq 0 \\ (R_{05} - R_{06})x_6 - x_7 \neq 0 \end{cases} \tag{62}$$

Proof of Theorem 1. If control laws u_1, u_2, and u_3, provided by (12), (29), and (46), hold conditions (62), then there exist the design parameters α, β, δ, the positive gains $k_1, k_2, k_3, k_4, k_5, k_6$, and the degree of nonlinearity used to prevent chattering ϕ_1, ϕ_2, ϕ_3; as a result, the closed-loop DCMG-system (1) is exponentially stable. □

Finally, we may define the creative Lyapunov function for the total DCMG system (1) $V_{1,2,3,4,5,6,7}(x) = V_{1,2}(x) + V_{3,5}(x) + V_4(x) + V_6(x) + V_7(x)$ as follows:

$$\begin{aligned} V_{1,2,3,4,5,6,7}(x) &= 2k_2|S_2| + \tfrac{1}{2}z_2^2 + \tfrac{1}{2}\left(k_1|S_2|^\alpha sgn\left(\tfrac{S_2}{\phi_1}\right) - z_2\right)^2 + \tfrac{R_1}{2}e_1^2 \\ &+2k_4|S_4| + \tfrac{1}{2}z_4^2 + \tfrac{1}{2}\left(k_3|S_4|^\beta sgn\left(\tfrac{S_4}{\phi_2}\right) - z_4\right)^2 + \tfrac{R_2C_2}{2}e_3^2 + \tfrac{R_3C_3}{2}e_5^2 \\ &2k_6|S_6| + \tfrac{1}{2}z_6^2 + \tfrac{1}{2}\left(k_5|S_6|^\delta sgn\left(\tfrac{S_6}{\phi_3}\right) - z_6\right)^2 + \tfrac{1}{2}e_7^2 \end{aligned} \tag{63}$$

Its time derivative is then

$$\begin{aligned} \dot{V}_{1,2,3,4,5,6,7}(x) \quad &= -\tfrac{1}{2|S|^\alpha}X_{1,2}^T Q_{1,2} X_{1,2} - \tfrac{1}{2|S|^\beta}X_4^T Q_4 X_4 \\ &-\tfrac{1}{2|S|^\delta}X_6^T Q_6 X_6 - e_3^2 - e_5^2 - e_7^2 \end{aligned} \tag{64}$$

7. Simulations Results

The DCMG was created with the SimPowerSystem toolbox from Matlab/Simulink. Table 5 shows the parameters that have been utilized in the DCMG. The DC-bus is modeled in this simulation as a capacitor; the intended voltage on the DC-bus is V_{DCref} = 40 V and the switching frequency is 100 kHz. The PV generator is constituted by two modules in series; the number of cells per module is sixty and there are four parallel connected strings. The voltage in open-circuit V_{OC} = 363 V, current in short-circuit I_{OC} = 8 A, voltage at the maximum power point V_{mpp} = 17 V, current at the maximum power point I_{mpp} = 7.1 A, and the power in the maximum point per module P_{mp} =120.7 W.

Table 5. The simulated DCMG parameters.

R_{02},R_{04},R_{06}	45 mΩ
R_{01},R_{03},R_{05}	44 mΩ
R_1,R_2,R_3	14 mΩ
C_1,C_2,C_3	4700 µF
C_{DC}	1500 µF
L_1,L_2,L_3	100 µH

The suggested supercapacitor bank has a total capacitance of 29 F and a rated voltage of 32 V. The battery is an Li-ion battery with a 24 V nominal voltage. The maximum charge current is 17.5 A, while the maximum discharge current is 30 A. The current capacity is 14 Ah.

The major aim is to show that the suggested control approach performs effectively in circumstances of variable solar irradiation and load fluctuations. It is planned that the voltage of the DC-bus will be regulated with a subsystem battery and subsystem SC in such a way that the SC will rapidly provide the elements of the needed DC-bus voltage compensated current, while the subsystem battery device will provide the slow variable components.

The gains utilized in the simulated nonlinear controllers are as follows: $a_2 = 0.1$, $a_4 = 0.45, a_6 = 0.13, \alpha = 0.2, \beta = 0.5, \delta = 0.2$, $k_1 = 960$, $k_2 = 1000$, $k_3 = 900$, $k_4 = 1000 k_5 = 750$, $k_6 = 900$, $\phi_1 = 0.6$, $\phi_2 = 0.9$, and $\phi_3 = 0.8$. To validate the effectiveness of the solar energy subsystem, the suggested controller (12) has been simulated. Figure 9 depicts the power generated by the PV subsystem in relation to the desired voltage V_{C1ref} determined from the MPPT algorithm, which assures the maximum power from the solar energy subsystem under variable environmental circumstances.

To create the battery and SC reference currents (I_{L2ref} and I_{L3ref}), as well as the energy management system, the fuzzy logic system was applied. Figure 10 shows the varying DC load current used for the controllers. The suggested controllers in Equations (29) and (46) have also been tested to ensure that the battery current I_{L2} and SC current I_{L3} are tracked under load demands and are high.

Figures 11 and 12 show how the proposed controllers track the battery and SC current. The discontinuous structure of the PV subsystem energy, along with the load changes, cause the rapid variations in the battery reference current. The load need reduces from t = 10 until t = 14 s, but the intermittent power provided by the PV subsystem also declines, thus the battery and SC satisfy the load requirement.

Figure 13 shows that the suggested controllers meet the goal of DC-bus voltage management with peak overshoot and less misses, resulting in the greatest power contribution from the PV system, battery, and SC. It is possible to evaluate the DC-bus voltage tracked to its desired value without overrun.

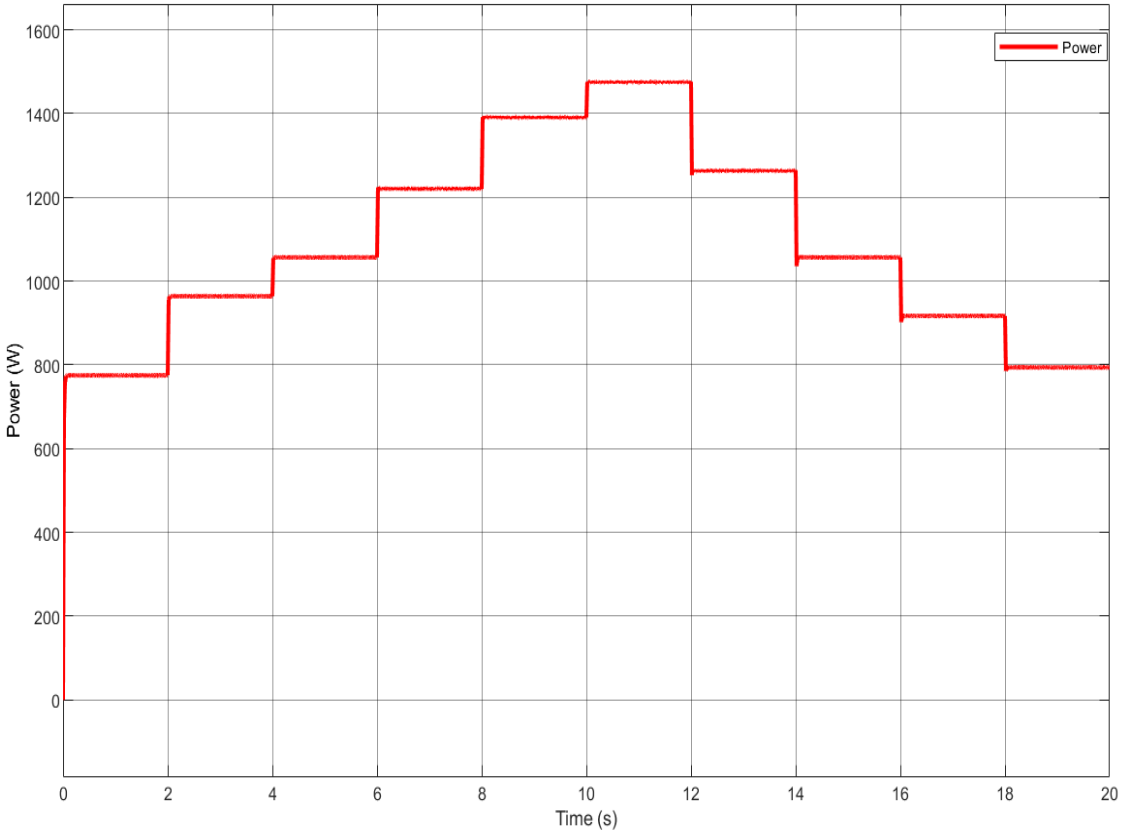

Figure 9. Evolution of PV power.

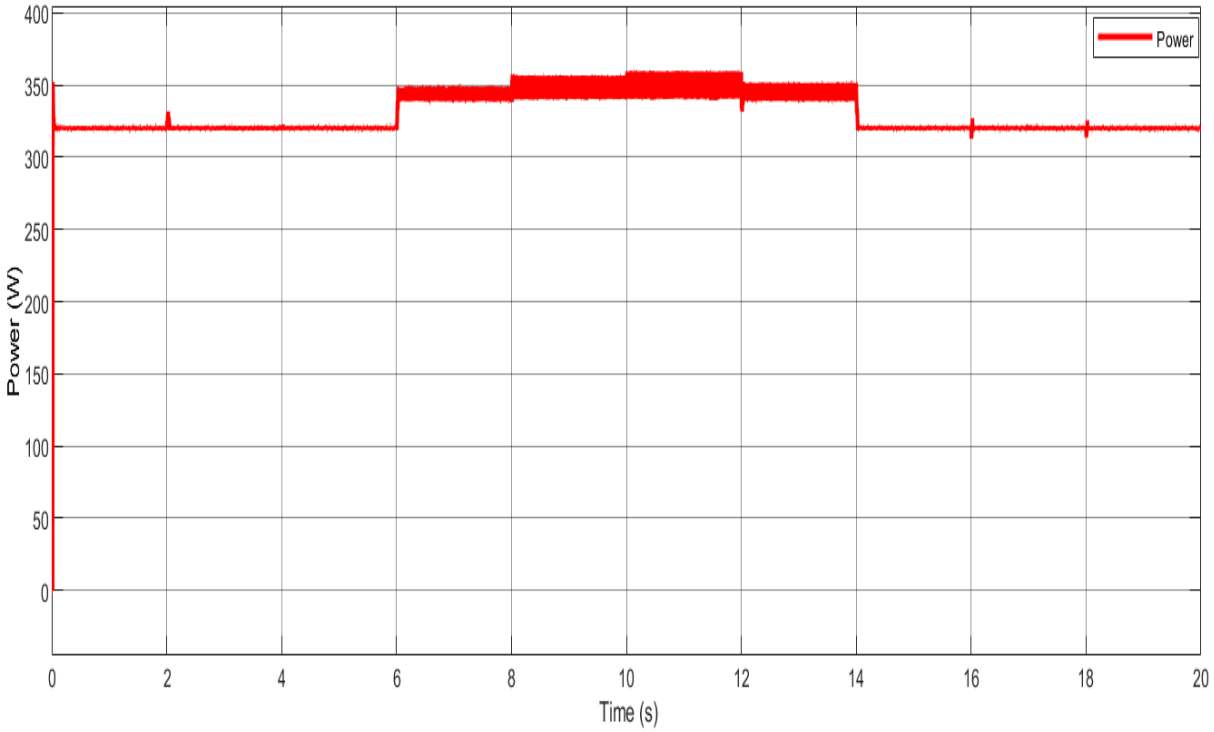

Figure 10. Evolution of the load power.

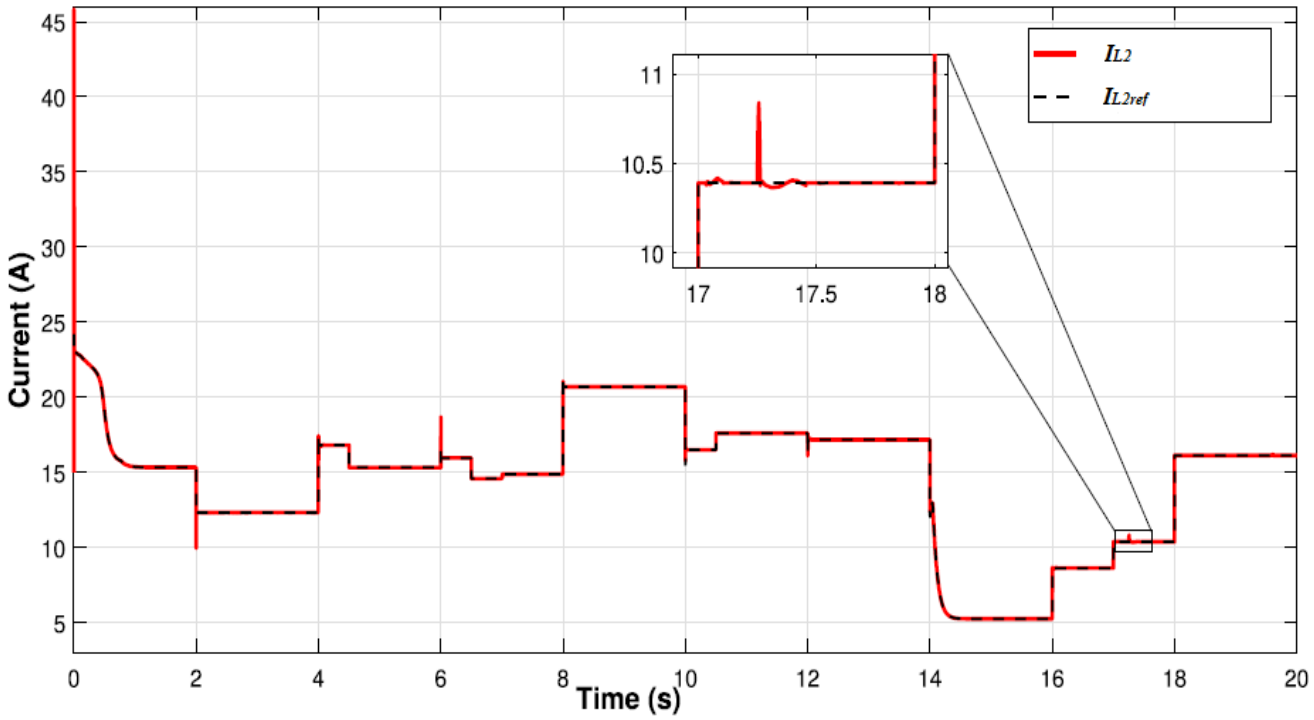

Figure 11. Evolution of the battery current (I_{L2} and I_{L2ref}).

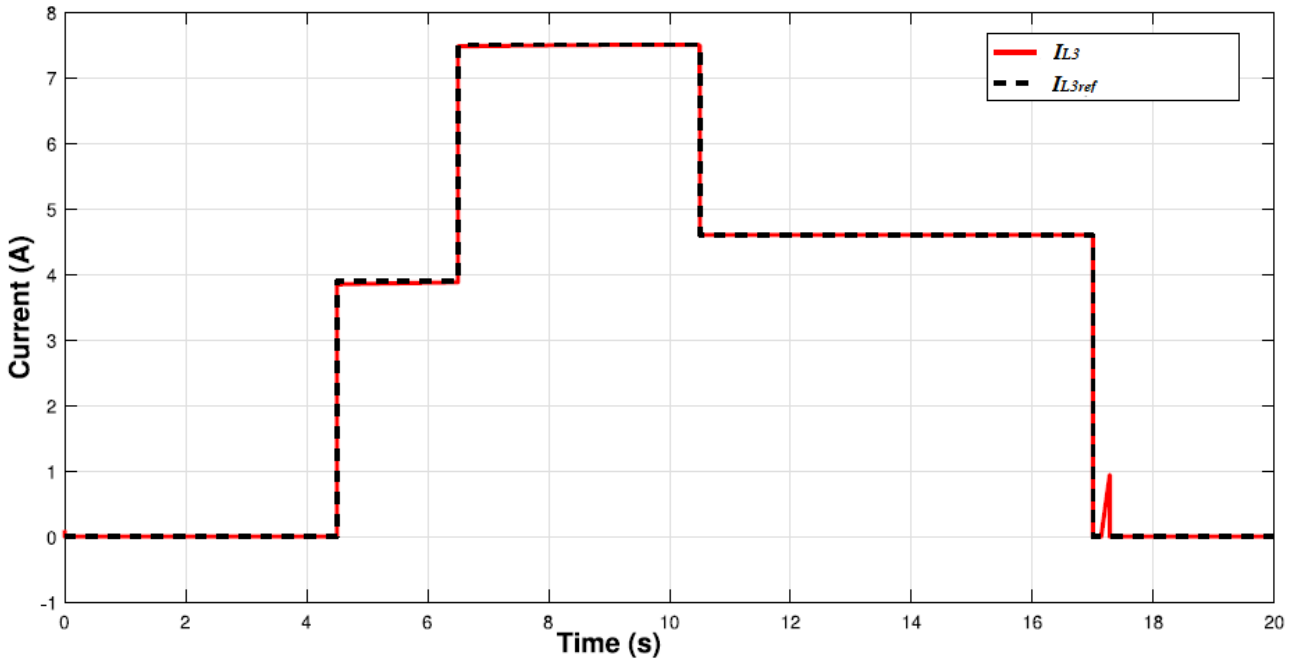

Figure 12. Evolution of the SC current (I_{L3} and I_{L3ref}).

Figure 11 shows one of the overshoots during t = 6 s with a maximum voltage at 40.5 V, yet it is within the allowed range of values, since the voltage of the DC-bus has been monitored at all times. The overshoot and misses of the target are caused by variations in the load demand and produced power.

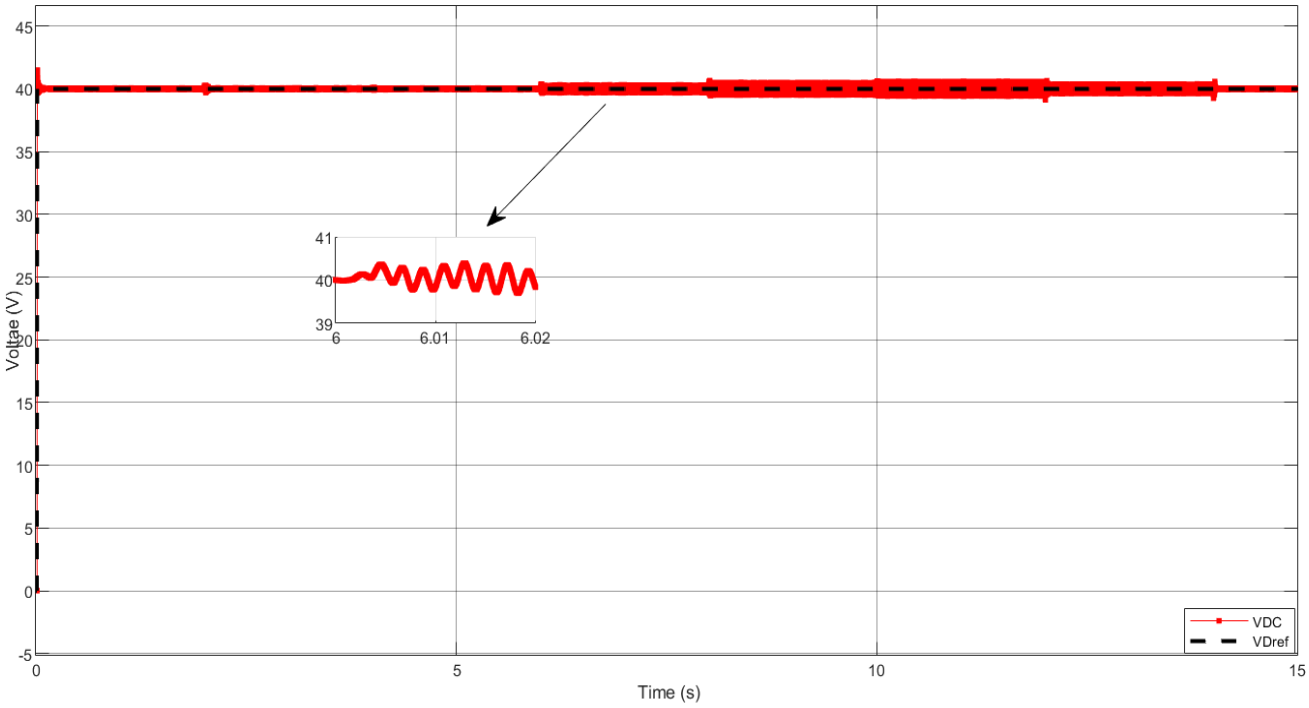

Figure 13. Evolution of the DC bus voltage (V_{DC} and V_{DCref}).

8. Conclusions

This research study proposed a renewable energy source consisting of photovoltaic (PV) panels, a battery, and a supercapacitor (SC), combined with a DC bus. Sliding-mode controllers were employed to manage the power sources, allowing them to operate at their maximum power point tracking (MPPT) capacity, while maintaining the power balance between the PV and the energy storage system (ESS). To balance the load and generation, a fuzzy logic-based energy management system was developed. Using a neural network, the maximum power points for the PV were determined. The proposed control technique allows for power management between the battery, SC, and PV to meet the load requirements. Lyapunov analysis was used to confirm the global asymptotic stability of the DC microgrid (DCMG) system. To validate the performance of the proposed framework, the SMC and FLS-based energy management system was simulated. Numerical simulations of the DC microgrid with the suggested controllers demonstrated excellent dynamic performance under various operating conditions caused by significant random changes in power generation and consumption. In the future, this work could be extended to include an AC-DC microgrid, and wind sources could be integrated into the microgrid.

Author Contributions: Conceptualization, K.J., M.J., A.M., A.J.B. and W.B.; Methodology, K.J., M.J., A.M., A.J.B. and W.B.; Software, K.J. and W.B.; Validation, K.J., M.J., A.J.B. and W.B.; Formal analysis, K.J., M.J., A.M., A.J.B. and W.B.; Investigation, K.J., M.J. and W.B.; Resources, K.J., A.M. and A.J.B.; Data curation, K.J. and A.M.; Writing—original draft, K.J. and M.J.; Writing—review & editing, A.M., A.J.B. and W.B.; Supervision, W.B. All authors have read and agreed to the published version of the manuscript.

Funding: This research was funded by Taif University, Taif, Saudi Arabia (TU-DSPP-2024-70).

Data Availability Statement: The original contributions presented in the study are included in the article, further inquiries can be directed to the corresponding author.

Acknowledgments: This research was funded by Taif University, Saudi Arabia, Project Nº (TU- DSPP-2024-70).

Conflicts of Interest: The authors declare no conflict of interest.

Nomenclature

DG	Distributed Generation
RES	Energy Renewable Source
ESS	System Energy Storage
SoC	State of Charge
SMC	Sliding-ModeController
SF	Sliding Surface
SE	Solar Energy
DC	Direct Current
AC	Alternating Current
MG	Microgrid
DCMG	Direct Current Microgrid
MPPT	Maximum Power Point Tracking
SC	Supercapacitor
PWM	Pulse Width Modulation
PV	Photovoltaic
PI	Proportional Integral
FLS	Fuzzy Logic System
PWM	Pulse Width Modulation
ANN	Artificial Neural Network

References

1. Zeng, B.; Zhang, J.; Yang, X.; Wang, J.; Dong, J.; Zhang, Y. Integrated planning for transition to low-carbon distribution system with renewable energy generation and demand response. *IEEE Trans. Power Syst.* **2013**, *29*, 1153–1165. [CrossRef]
2. Rahbar, K.; Chai, C.C.; Zhang, R. Energy cooperation optimization in microgrids with renewable energy integration. *IEEE Trans. Smart Grid.* **2016**, *9*, 1482–1493. [CrossRef]
3. Loh, P.C.; Li, D.; Chai, Y.K.; Blaabjerg, F. Hybrid AC-DC microgrids with energy storages and progressive energy flow tuning. *IEEE Trans. Power Electron.* **2012**, *28*, 1533–1543. [CrossRef]
4. Guerrero, J.M.; Chandorkar, M.; Lee, T.L.; Loh, P.C. Advanced control architectures for intelligent microgrids—Part I: Decentralized and hierarchical control. *IEEE Trans. Ind. Electron.* **2012**, *60*, 1254–1262. [CrossRef]
5. Khorsandi, A.; Ashourloo, M.; Mokhtari, H.; Iravani, R. Automatic droop control for a low voltage DC microgrid. *IET Gener. Transm. Distrib.* **2016**, *10*, 41–47. [CrossRef]
6. Bevrani, H.; Francois, B.; Ise, T. *Microgrid Dynamics and Control*, 1st ed.; John Wiley and Sons: Hoboken, NJ, USA, 2017.
7. Nair, D.R.; Nair, M.G.; Thakur, T. A Smart Microgrid System with Artificial Intelligence for Power-Sharing and Power Quality Improvement. *Energies* **2022**, *15*, 5409. [CrossRef]
8. Liu, J.; Zhang, W.; Rizzoni, G. Robust stability analysis of DC microgrids with constant power loads. *IEEE Trans. Power Syst.* **2017**, *33*, 851–860. [CrossRef]
9. Li, X.; Guo, L.; Zhang, S.; Wang, C.; Li, Y.W.; Chen, A. Observer-based DC voltage droop and current feed-forward control of a DC microgrid. *IEEE Trans. Smart Grid.* **2017**, *9*, 5207–5216. [CrossRef]
10. Etemadi, A.H.; Davison, E.J.; Iravani, R. A generalized decentralized robust control of islanded microgrids. *IEEE Trans. Power Syst.* **2014**, *29*, 3102–3113. [CrossRef]
11. Kumar, M.; Srivastava, S.; Singh, S. Control strategies of a DC microgrid for grid connected and islanded operations. *IEEE Trans. Smart Grid.* **2015**, *6*, 1588–1601. [CrossRef]
12. Babazadeh, M.; Karimi, H. A robust two-degree-of-freedom control strategy for an islanded microgrid. *IEEE Trans. Power Deliv.* **2013**, *28*, 1339–1347. [CrossRef]
13. Du, Z.; Kao, Y.; Karimi, H.R.; Zhao, X. Interval type-2 fuzzy sampled-data H∞ control for nonlinear unreliable networked control systems. *IEEE Trans. Fuzzy Syst.* **2019**, *28*, 1434–1448. [CrossRef]
14. Iovine, A.; Siad, S.B.; Damm, G.D.; Santis, E.; Benedetto, M.D. Nonlinear control of a DC microgrid for the integration of photovoltaic panels. *IEEE Trans. Autom. Sci. Eng.* **2017**, *14*, 524–535. [CrossRef]
15. Hassan, M.A.; Li, E.p.; Li, X.T.; Li, C.; Duan, S. Adaptive passivity-based control of dc–dc buck power converter with constant power load in dc microgrid systems. *IEEE J. Emerg. Sel. Top Power Electron.* **2018**, *7*, 2029–2040. [CrossRef]
16. Roy, T.K.; Mahmud, M.A.; AMT, O.; Haque, M.E.; Muttaqi, K.M.; Mendis, N. Nonlinear adaptive backstepping controller design for islanded DC microgrids. *IEEE Trans. Ind. Appl.* **2018**, *54*, 2857–2873. [CrossRef]
17. Baghaee, H.R.; Mirsalim, M.; Gharehpetian, G.B.; Talebi, H.A. A decentralized power management and sliding mode control strategy for hybrid AC/DC microgrids including renewable energy resources. *IEEE Trans. Ind. Inf.* **2018**, *99*, 1–10. [CrossRef]
18. Benchaib, A. *Advanced Control of AC/DC Power Networks: System of Systems Approach Based on Spatio-Temporal Scales*; Wiley-ISTE: London, UK, 2015.

19. Kundur, P.; Paserba, J.; Ajjarapu, V.; Andersson, G.; Bose, A.; Canizares, C. Definition and classification of power system stability IEEE/CIGRE joint task force on stability terms and definitions. *IEEE Trans. Power Syst.* **2004**, *19*, 1387–1401.
20. Siad, S.; Damm, G.; Dol, L.G.; Bernardinis, A. Design and control of a dc grid for railway stations. In Proceedings of the PCIM Europe 2017, International Exhibition and Conference for Power Electronics, Intelligent Motion, Renewable Energy and Energy Management, Nuremberg, Germany, 16–18 May 2017; pp. 1–8.
21. Merdassi, A. *Modellisation Automatique pour l'Electronique de Puissance*; Editions Universitaires Européennes: Chisinau, Moldova, 2010.
22. Bhatia, R.S.; Singh, B.; Jain, D.K.; Jain, S.P. Battery energy storage system based power conditioner for improved performance of hybrid power generation. In Proceedings of the Joint International Conference on Power System Technology and IEEE Power India Conference, New Delhi, India, 12–15 October 2008; pp. 1–6.
23. Jouili, K.; Adel, M. Nonlinear Lyapunov control of a photovoltaic water pumping system. *Energies* **2023**, *16*, 2241. [CrossRef]
24. Tse, C.K.; Bernardo, M.D. Complex behavior in switching power converters. *Proc. IEEE.* **2002**, *90*, 768–781. [CrossRef]
25. Jouili, K.; Benhadj Braiek, N. A gradient descent control for output tracking of a class of non-minimum phase nonlinear systems. *JART J. Appl. Res. Technol.* **2016**, *14*, 383–395. [CrossRef]
26. Moreno, J.A.; Osorio, M. A Lyapunov approach to second-order sliding mode controllers and observers. In Proceedings of the 2008 47th IEEE Conference on Decision and Control, Cancun, Mexico, 9–11 December 2008; pp. 2856–2861.
27. Jouili, K.; Belhadj, W. Robust stabilization for uncertain non-minimum phase switched nonlinear System under arbitrary switchings. *Symmetry* **2023**, *15*, 596. [CrossRef]
28. Jouili, K.; Jerbi, H.; Braiek, B.N. An advanced fuzzy Logic gain scheduling trajectory control for nonlinear systems. *JPC J. Process Control* **2010**, *20*, 426–440. [CrossRef]